JOURNAL OF GEOPHYSICAL RESEARCH, VOL. 103, NO. A5, PAGES 9249–9260, MAY 1, 1998

Precipitation of radiation belt electrons by magnetospherically reflected whistlers

J. L. Ristić-Djurović
Vinča Institute of Nuclear Science, Belgrade, Yugoslavia

T. F. Bell and U. S. Inan
STAR Laboratory, Stanford University, Stanford, California

Abstract. We use a test particle simulation model based on gyro-averaged equations of motion to study the influence of oblique magnetospherically reflected (MR) whistlers on the near-loss-cone distribution function of radiation belt electrons. We find that MR whistlers originating in lightning can resonantly interact with radiation belt electrons over a broad range of L shells and precipitate higher energy electrons from lower L shells. Electrons in the energy-range of 1 to 2.6 MeV are precipitated from $L = 2$, whereas from $L = 4$ the precipitated electron energy range is 150–220 keV. The precipitated differential electron flux, due to this interaction, is higher for higher L shells, and the maximum value ranges from $\Phi_{E_{prec}}(1.11\ \text{MeV}) = 5.2 \times 10^{-4}$ electrons cm^{-2} s^{-1} keV^{-1} at $L = 2$ to $\Phi_{E_{prec}}(173\ \text{keV}) = 4.6 \times 10^{-1}$ electrons cm^{-2} s^{-1} keV^{-1} at $L = 4$. The lifetimes of radiation belt electrons in a given magnetic flux tube around the L shell on which the interaction takes place are found to be of the order of several days, comparable to lifetimes corresponding to electron loss induced by hiss, which was heretofore assumed to be the dominant loss mechanism [*Lyons et al.*, 1972]. The minimum electron lifetimes vary from 2.4 days for 1.11 MeV electrons at $L = 2$ to 4.6 days for 173 keV electrons at $L = 4$.

1. Introduction

Past investigations of resonant whistler mode wave–particle interactions have recognized their importance in the loss of radiation belt electrons [e.g., *Dungey*, 1963] and have evolved in essentially two directions depending on the coherence of the wave. When interacting with broadband and incoherent whistler mode waves through cyclotron resonance, individual particles are subject to a series of random pitch angle scattering so that for a population of particles the interaction can be viewed as a diffusion process. The cyclotron resonant interaction of a distribution of particles with an incoherent whistler mode wave can thus be studied via diffusion coefficients formulated in the particle's equatorial pitch angle space [*Roberts*, 1966]. This approach was used by *Kennel and Petschek* [1966], *Lyons et al.* [1972], *Lyons and Thorne* [1973], *Spjeldvik and Thorne* [1975], and others to study interactions of radiation belt particles with a class of incoherent magnetospheric signals known as plasmaspheric hiss. Note that past studies based on the diffusion coefficient approach have included interactions between radiation belt electrons and oblique whistler mode waves [*Roberts*, 1969; *Lyons et al.*, 1971].

The physics of wave-particle interactions for the case of coherent and narrow-band whistler mode waves is fundamentally different. During the interaction with a coherent wave, individual particles are not scattered randomly; instead, they stay in resonance with the wave long enough for the particle's pitch angle to be substantially changed. This nonlinear interaction has been extensively studied for ducted whistlers by the means of a test particle simulation model [*Inan*, 1977; *Inan et al.*, 1978, 1982; *Chang*, 1983; *Chang and Inan*, 1983a,b; *Chang et al.*, 1983] including direct comparisons with experimental data [*Inan et al.*, 1985a; 1989]. A good review of this approach and a comparison between interactions with coherent versus incoherent waves is given by *Inan* [1987].

Experimental observations have shown that ionospheric effects of precipitated electrons, such as subionospheric VLF perturbations, X ray emissions, or photoemissions can often be correlated with natural ducted VLF waves (whistlers, chorus emissions, noise bursts, etc.) [*Rosenberg et al.*, 1971; *Helliwell et al.*, 1973; *Foster and Rosenberg*, 1976; *Lohrey and Kaiser*, 1979; *Helliwell et al.*, 1980; *Mende et al.*, 1980; *Rosenberg et al.*, 1981; *Dingle and Carpenter*, 1981; *Carpenter and LaBelle*, 1982]. In particular, the ionospheric signatures of energetic electrons scattered out of the radiation belts in cyclotron resonant interactions with lightning–generated ducted (i.e., parallel propagating) whistlers have been studied in detail [e.g., *Chang and Inan*, 1985] and are now commonly observed [*Inan et al.*, 1990; *Burgess and Inan*, 1993, and references therein].

As a measure of the effectiveness of this interaction involving ducted waves, precipitated energetic electron fluxes have been theoretically estimated and compared with experimental data [*Inan et al.*, 1985b; *Inan and Carpenter*, 1987; *Inan et al.*, 1989]. However, the bulk of the wave energy injected into the magnetosphere by lightning discharges propagates in the nonducted mode. In this mode, the wave normal vec-

Paper number 97JA03724
0148-0227/98/97JA-03724$09.00

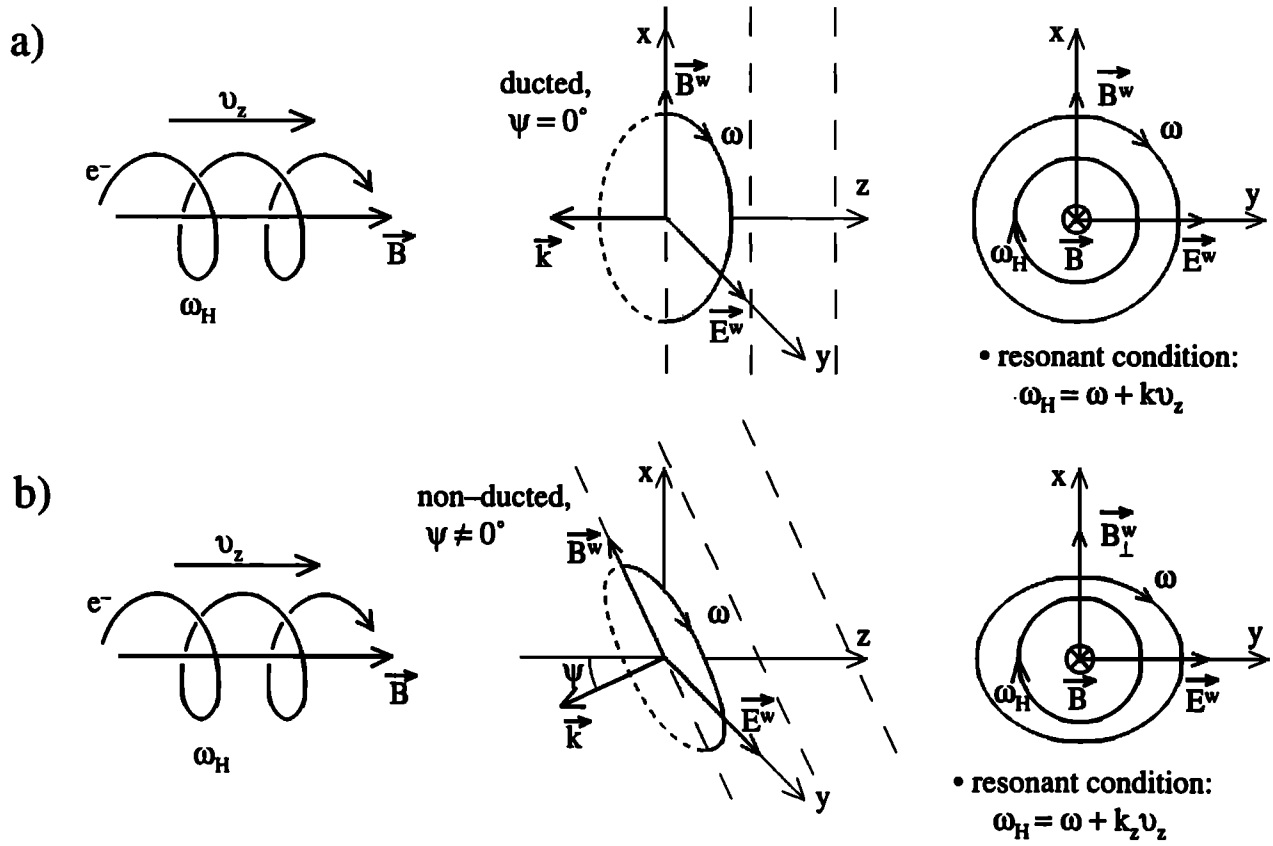

Figure 1. Electron-wave cyclotron resonance. Cyclotron resonant interactions between gyrating electrons and right hand elliptically polarized waves are schematically shown and resonant conditions given for the interaction with (a) ducted ($\psi = 0^0$), circularly polarized wave and b) oblique ($\psi > 0^0$), elliptically polarized wave.

tor is generally oriented at an oblique angle with respect to the Earth's magnetic field, and the waves can propagate freely across this field. The overall effect of nonducted coherent whistler mode waves on radiation belt electron precipitation is yet to be ascertained.

The first attempt to study resonant interactions between radiation belt electrons and oblique whistler mode waves using a test particle approach was made by *Jasna et al.* [1992]. Using gyro-averaged equations of motion for a test electron, a test particle trajectory simulation model was developed and used to study precipitation of suprathermal (100 eV) electrons by oblique whistler waves. This result was put in perspective by its comparison with the scattering of energetic (100 keV) electrons by both ducted and nonducted waves.

The geometry of cyclotron resonance between gyrating electrons and elliptically polarized components of both ducted and nonducted whistler mode waves is schematically illustrated in Figure 1. The electrons rotate in the same direction as the electric and magnetic fields of the right-hand elliptically polarized waves (in general, an oblique whistler mode wave is elliptically polarized, but for the special case of ducted waves ($\psi = 0°$) the polarization is circular). If the rate of rotation of the electron and wave are matched, the wave fields appear to have stationary phase in the reference frame of the electron.

The test particle trajectories illustrate the detailed dynamics of the electron–wave interaction and the resultant electron pitch angle and velocity scattering, as well as the duration of the interaction and its dependence on electron and wave input parameters (initial electron velocity, wave frequency and wave normal angle). However, full distribution modeling is required to assess the effects of the oblique whistler–electron interactions on the radiation belt electron population and to quantitatively evaluate these resulting effects in terms of measurable quantities such as precipitated electron fluxes and lifetimes. The development and application of a test particle model of interaction between oblique whistler mode waves and a full distribution of radiation belt electrons is the subject of this paper in which we provide a first estimate of the effectiveness of nonducted whistlers in precipitating particles.

2. Magnetospherically Reflected Whistlers

Nonducted (oblique) whistler mode waves originating in lightning discharges are often found to undergo multiple reflections between hemispheres. These reflections occur at points where the wave frequency matches the local lower hybrid resonance frequency [*Edgar*, 1976]. Figure 2 shows an example of magnetospherically reflected (MR) whistler components observed on the Polar spacecraft. The format is one of a typical frequency versus time spectrogram with the density of the shading representing the intensity of the recorded signal. A single lightning discharge gives rise to a series of MR whistler components numbered from 1 to 8 in Figure 2. Component 1 propagates directly from the grond to the spacecraft. Component 2 reflects once in the con-

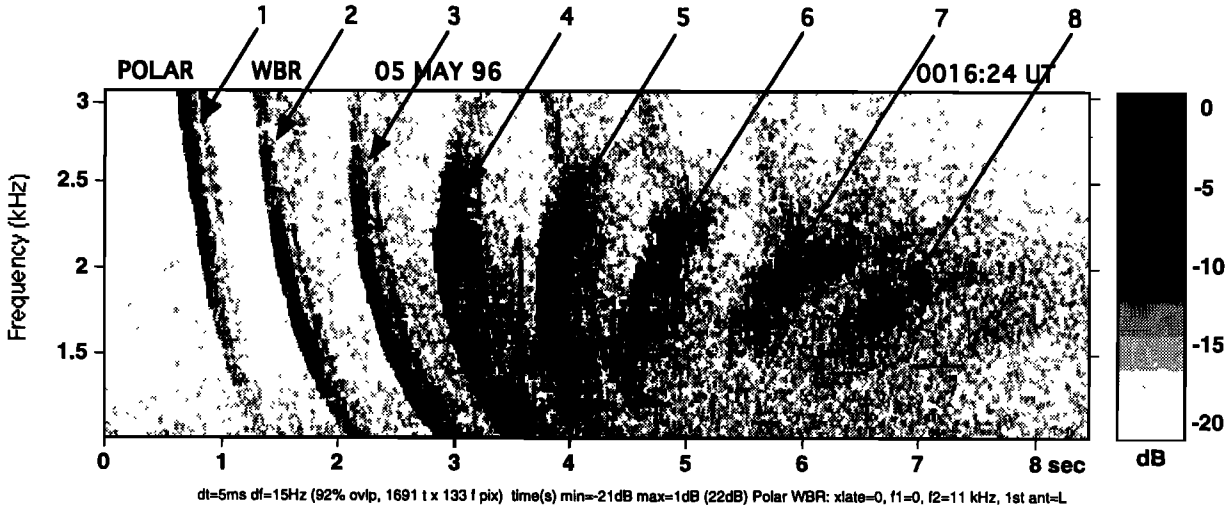

Figure 2. An example of MR whistler components observed on the Polar spacecraft. A single lightning discharge gives rise to a series of MR whistler components numbered from 1 to 8.

jugate hemisphere before reaching the spacecraft, and each subsequent component of number N reflects N - 1 times before reaching the spacecraft. Note that the wave intensity in the first few components is distributed over a wide frequency range, but in the final components the wave becomes more monochromatic and its intensity is confined to a narrow frequency range ($\sim$ 500 Hz). Although the total duration of the MR event is $\sim$8 s for the case shown, MR whistlers are known to last for as long as 100 s [*Draganov et al.*, 1992].

Both ducted and MR (oblique) whistlers are generated by lightning discharges (Figure 3). It should be noted that nonducted whistlers do not require the presence of any specific density structures (e.g., ducts) for their propagation. They generally occupy larger regions of the magnetosphere [*Sonwalkar and Inan*, 1993]. On this basis, although the statistics of the occurrence rates of nonducted whistlers are not well documented, it may safely be assumed that they occur at least as often as ducted whistlers and may be excited by every lightning discharge.

Under some circumstances, nonducted whistlers may be strongly attenuated by landau damping [*Thorne and Horne*, 1994], although this is generally not the case for ducted whistlers. The ducted whistler rate depends on the time of the year and time of the day, and at Port Lockroy ($L \sim$ 2.5), Antarctica, it was found to vary from 0.3 whistlers per minute for an average summer day to 22 whistlers per minute for an average winter night [*Burgess and Inan*, 1993]. For an extremely active day, the ducted whistler rate can be as high as 195 whistlers per minute, but year-round average is 6 whistlers per minute.

The magnetospheric reflection of oblique whistler mode waves can be effectively studied by raytracing. Here we utilize the Stanford VLF ray tracing code for cold plasmas [e.g., see *Inan and Bell*, 1977] and assume a dipole ambient magnetic field and a diffusive equilibrium model for the cold plasma density, with equatorial profile the same as shown by *Jasna et al.* [1990, Figure 3.]. The example in Figure 4 shows a $f = 0.33$ kHz wave injected vertically upward from the southern hemisphere at $L = 2$. The ray travels vertically upward reflecting back and forth between the hemispheres as expected and eventually settles down at $L \cong 4$. More extensive ray tracing studies [*Draganov et al.*, 1992] show that the L shell at which the whistler wave settles down depends strongly on the wave frequency but is relatively independent of the injection latitude or initial wave propagation direction. The frequency of the whistler wave versus L shell of settlement as obtained from ray tracing is plotted in Figure 5. It should be noted that under some circumstances

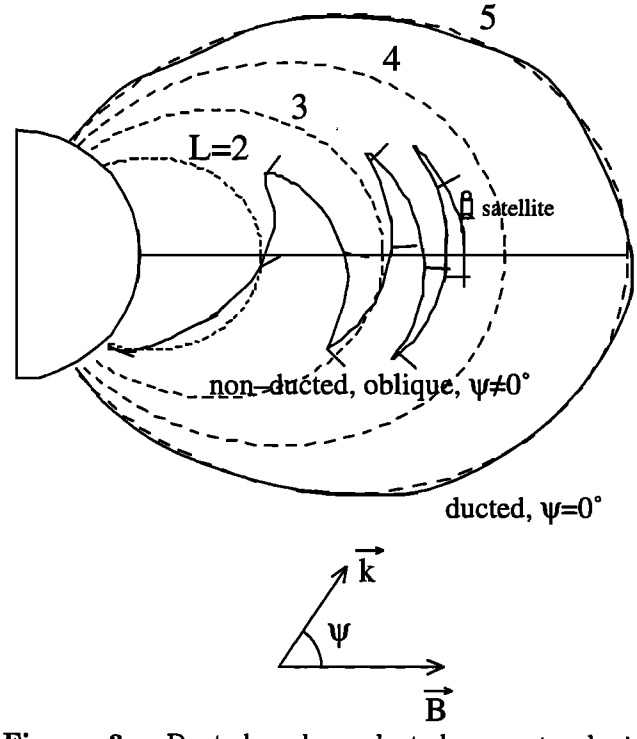

Figure 3. Ducted and nonducted magnetospheric waves. Ducted waves travel within the background plasma density enhancements called ducts. Their wave normal angle is approximately parallel to the magnetic field line, they penetrate through the atmosphere and are detected on the ground. Nonducted waves propagate with their wave normal at a substantial angle with respect to the magnetic field line; they are typically reflected within the magnetosphere before they reach the ionosphere and can typically be detected only in situ.

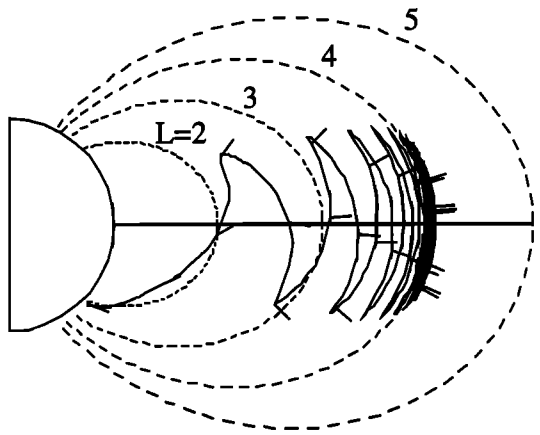

Figure 4. Sample raypath for an MR signal. The ray path for a $f = 0.33$ kHz wave injected at 400 km altitude, vertically upward from the southern hemisphere at $L = 2$, propagating to higher L shells by reflecting back and forth between hemispheres and eventually settling down at $L \approx 4$.

the ray tracing is more accurately carried out using a hot plasma code [*Thorne and Horne*, 1994].

To summarize, MR whistlers are oblique whistler mode waves injected into the magnetosphere by lightning, they can endure in the magnetosphere for as long as 100 s each, and after several (5–6) reflections the ray paths settle down into a multiply reflecting pattern at an L shell uniquely corresponding ($f \approx f_{LHR}$) to the signal frequency. Thus, at any given L shell, we can expect accumulation of oblique whistler mode wave energy at the corresponding frequency. This phenomenon may be responsible for the intensification of the wave energy commonly observed at the lower cut off frequency ($f \sim f_{LHR}$) of the ubiquitous lower-hybrid-resonance noise band [*Laaspere et al*, 1971]. The wave normal angle of the multiply reflecting waves slowly varies with latitude along the field line in a particular manner as disclosed by raytracing. As such, these multiply reflecting waves, continuously present along the given L shell constitute a narrowband wave which can resonantly interact with the radiation belt electrons. It should be noted that the wave distribution along the field line consists of a superposition of multiply reflecting waves. In the following, we use a test particle simulation to represent the interactions of a distribution of electrons with these continuously present nearly monochromatic MR whistlers, the wave normal angle of which vary along the field line as described by raytracing. Our assumption of a monochromatic wave with specified phase variation amounts to considering one of the many multiply reflecting wave components, the superposition of which may generate standing wave patterns and slow variations in wave phase.

3. Initial Conditions and Assumptions

In the inner magnetosphere ($L \leq 6$), the background "cold" plasma consists of isothermal mixture of electrons and positive ions (H^+, He^+, and O^+) forming a diffusive equilibrium along the magnetic field lines [*Angerami and Thomas*, 1964]. The variation along the magnetic field lines of the electron density for the diffusive equilibrium model of the cold plasma density is given by *Park* [1972]. In the region of our interest (inner magnetosphere), the Earth's magnetic field lines are not significantly distorted by the solar wind and for our purposes can be modeled using a centered dipole tilted with respect to the rotational axis by ~11°.

We describe the initial electron distribution function in a manner similar to that of *Inan et al.* [1978] and *Chang and Inan* [1985]. We assume that radiation belt electrons are uniformly distributed in the electron pitch angle space between the loss cone angle α_{lc} and $\pi/2$ and with an energy dependence of the form

$$f_E(E) \propto E^{-3}$$

based on experimental data [*Schield and Frank*, 1970]. We can alternatively express the distribution in terms of the electron velocity

$$f_v(v) = \frac{A}{v^6} \quad .$$

Since the energetic electron population is commonly described and measured in terms of the differential energy spectrum $\Phi_{E_{diff}}(E)$, the constant A in the above expression is chosen such that the corresponding differential energy spectrum at $E = 1$ keV is

$$\Phi_{E_{diff}}(1 \text{ keV}) = 10^8 \frac{el}{\text{cm}^2 \text{ s keV str}}.$$

The corresponding value of the constant A is found to be

$$A = 7.034 \times 10^{26} \frac{el}{\text{s}^3 \text{ str}} \quad .$$

One of the fundamental assumptions of our test particle formulation is the fact that we neglect the effects on the wave of the distribution of energetic electrons. This means that we are assuming either that the currents stimulated in the particle population do not lead to significant damping or amplification of the wave or that this effect has been included in the model chosen for the wave structure. This approximation was also adopted in the test particle model studies of ducted wave–particle interactions [*Inan et al.*, 1982; *Chang and Inan*, 1985]. For ducted waves, wave growth is commonly observed to occur [e.g., *Helliwell*, 1988]; however, experimental and theoretical evidence suggest that the region of temporal growth of the wave is within a few degrees of the geomagnetic equator [*Helliwell*, 1967; *Helliwell and Katsufrakis*, 1974; *Tsurutani and Smith*, 1974; *Carlson et al.*, 1990]. Since the change in the wave amplitude structure occurs over a relatively small portion of the field line, the effect of such nonuniform amplitude variation on the total precipitated flux is likely to be negligible. For nonducted obliquely propagating waves, taking the wave as a prede-

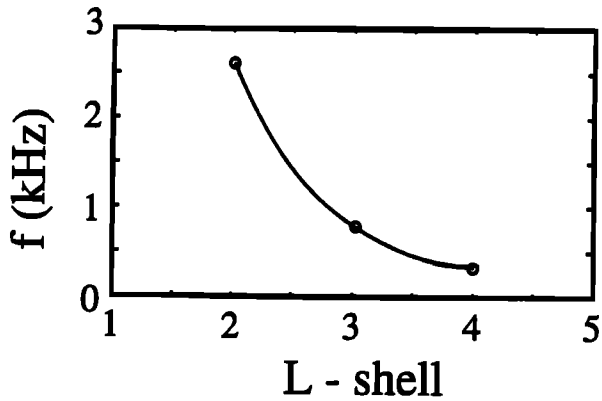

Figure 5. The frequency of the whistler wave versus L shell of settlement. This result is derived on the basis of simulated raypaths as shown on Figure 4.

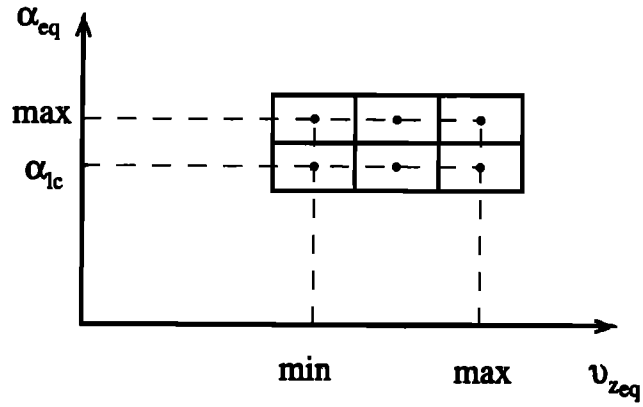

Figure 6. Velocity space cells. The portion of velocity space that is simulated here is divided into cells each of which is to be represented by test particles.

fined structure and neglecting the effects of the energetic particles on the wave is probably an even better approximation, since growth and emission triggering by non-ducted waves is observed much less often [*Bell et al.*, 1981].

In our modeling, then, we assume the wave to be monochromatic (single frequency), and propagating at a given angle ψ with respect to the magnetic field. With the wave frequency ω and wave normal angle ψ specified, all properties of the wave are defined in terms of the local cold plasma parameters. The properties (dispersion relation, polarization of the wave fields, group velocity) of the electromagnetic waves that are supported by the cold, infinite, homogeneous, collisionless plasma in the presence of the external homogeneous, static magnetic field B_o are derived from Maxwell's equations [*Stix*, 1962]. The magnetosphere is not a homogeneous medium since both the plasma density and magnetic field (and therefore plasma and cyclotron frequencies of the kth species, ω_{pk} and ω_{Hk}, respectively) vary in space. Fortunately, these spatial variations are generally small over the distance of the order of the wavelength, so that at any given point, the wave propagation can be represented using the slowly varying approximation (WKB) in which the wave is assumed to have the same characteristics as those of a wave traveling in a homogeneous medium having the same refractive index. The Poynting flux (power density) of the slowly varying wave was also assumed to be constant during its interaction with the radiation belt electrons, although the wave normal angle ψ was allowed to slowly vary with latitude as dictated by raytracing. The assumed constant Poynting flux value was used to calculate the wave field components at different points along the field line.

4. Electron Velocity Space

In general, electron velocity space is three dimensional. For the special case of electron motion in the Earth's magnetosphere, important features of the unperturbed particle motion can be described by only two velocity space coordinates, for example the equatorial pitch angle α_{eq} and the component of the particle velocity along the Earth's magnetic field line $v_{z_{eq}}$. We represent the full distribution function by a large number of individual test particles and infer the modification of the distribution from the simulated trajectories of each of the test particles in the presence of the wave. Once a new particle distribution is determined, measurable quantities such as differential (per unit particle energy) and total precipitated particle fluxes and radiation belt electron lifetimes, are easily derived.

Figure 6 shows $v_{z_{eq}} - \alpha_{eq}$ velocity space divided into cells. Note that in the absence of the wave, the trajectory of a test electron moving in the Earth's magnetic field would be a single point in $v_{z_{eq}} - \alpha_{eq}$ space. Because of the interaction with the wave, the electron trajectory in velocity space evolves along a curve with initial and final points corresponding to the initial and final velocity space coordinates. Since the wave forces acting on the particle are functions of the initial electron phase η (the third velocity coordinate that determines the direction of the electron velocity perpendicular to the Earth's magnetic field), electron trajectories and their final points in velocity space depend on the initial η [*Inan*,

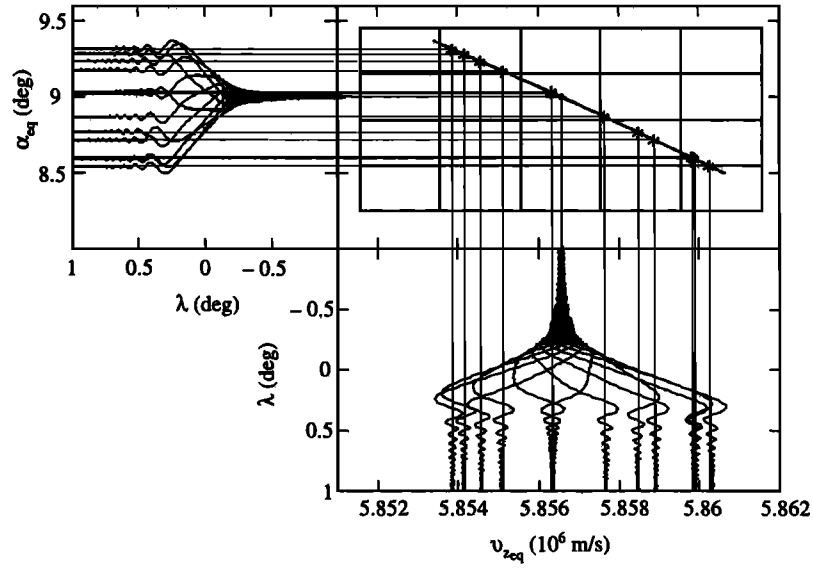

Figure 7. Test electron trajectories in the velocity space. Trajectories of the twelve test electrons with different initial phases, originating at the same initial point in velocity space are represented in velocity space as $\alpha_{eq}(V_{Z_{eq}})$ and as the velocity space coordinates dependence on geomagnetic latitude namely $\alpha_{eq}(\lambda)$ and $V_{Z_{eq}}(\lambda)$. All particles are introduced at $\lambda = -1^0$.

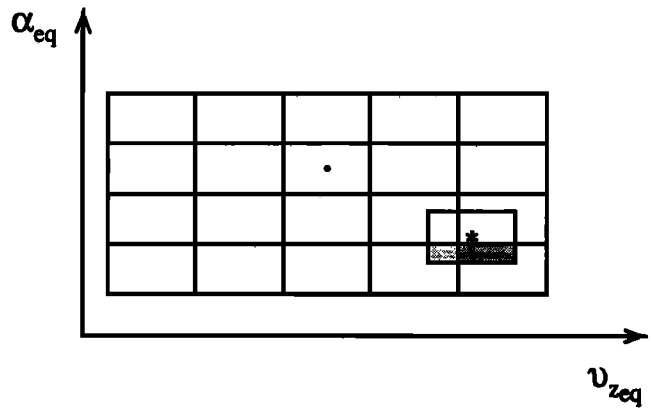

Figure 8. A single test electron scattering in velocity space. The schematics shows the initial and final point of the test electron trajectory in the velocity space. Electron population from the initial cell represented by the test electron is scattered into the four adjoining cells as represented by the cell corresponding to final point on the electron trajectory. The number of electrons scattered into any of the four adjoining phase cells is proportional to the area of the final cell that overlaps the corresponding cell. The initial point is shown by a dark circle; the final point by an asterisk.

1987; *Jasna et al.*, 1992]. Figure 7 shows twelve different electron trajectories corresponding to 12 electrons with different initial phases, originating at the same initial point in velocity space (i.e., having the same initial α_{eq} and $v_{z_{eq}}$. In view of this dependence of scattering on η, each cell in velocity space needs to be represented by a distribution of several test electrons with different initial phases. We choose 12 test electrons equally spaced in phase to represent a given cell based on the fact that the final scattering, i.e., the root-mean-square value of the final pitch angle change at the end of the resonant interaction, namely $\overline{\Delta\alpha_{eq_f}} = \sqrt{\langle\Delta\alpha_{eg}^2(\lambda_f)\rangle}$, (where averaging ($\langle\rangle$) is over the number of test electrons representing each cell) does not change significantly with further increase of the number of test electrons representing each cell. This choice of 12 test electrons limits the accuracy (the precision by which we can specify $\overline{\Delta\alpha_{eq_f}}$) of our calculations to $10^{-5\circ}$, well sufficient for our purposes here.

Since the goal of our study is to determine the modification of the electron distribution function in a single encounter with the wave (i.e., one pass) rather than the evolution of the distribution function with time during the interaction, and since we neglect the effects of the energetic particles on the wave, the initial and final points of the electron trajectory in velocity space determine the pitch angle scattering and the resultant change in the electron distribution function. Figure 8 shows the scattering of a single test electron in terms of the initial and final points in $v_{z_{eq}} - \alpha_{eq}$ space. The initial population of electrons as represented by any such test electron is then distributed into the four adjoining cells in proportion to the overlapping fractional area of the final cell. In other words, the fraction of the total number of electrons which populated the initial cell but which are scattered into any of the four cells adjoining the final point in $v_{z_{eq}} - \alpha_{eq}$ space is proportional to the area of the final cell, centered at the final point in $v_{z_{eq}} - \alpha_{eq}$ space, that overlaps each adjoining cell.

The modified electron distribution after a one-pass interaction with the wave is obtained using the scattering of all test electrons as described by the sample electron in Figure 8, weighed by the initial distribution function (electron density per velocity space volume) and its dependence on the velocity space coordinates (i.e., $f(v_{z_{eq}}, \alpha_{eq})$).

5. Particle and Energy Fluxes and Particle Lifetimes

The relationship between the particle distribution function $f(v_z, \alpha)$ and differential energy spectrum $\Phi_{E_{diff}}(E, \alpha)$ can be written as (see, for example, *Chang* [1983])

$$\Phi_{E_{diff}}(E,\alpha) = f(v_z,\alpha)\frac{v_z^2}{\cos^2\alpha}\frac{1}{m_e}\left(\sqrt{1-\frac{v_z^2}{c^2\cos^2\alpha}}\right)^3 .$$

To find the precipitated differential energy spectrum at atmospheric altitudes, we multiply with the correction factor to take into account the reduction of the flux tube volume element and integrate

$$\Phi_{E_{prec}}(E) = \pi\frac{\sqrt{1+3\sin^2\lambda_{at}}}{\cos^6\lambda_{at}}\int_{\alpha_{eq}=0}^{\alpha_{lc}}\Phi_{E_{diff}}(E,\alpha_{eq})\sin(2\alpha_{eq})\,d\alpha_{eq} .$$

The precipitated differential energy flux is defined as

$$dQ = E\Phi_{E_{prec}}(E)dE$$

and the total precipitated energy flux can be found

$$Q = \int_E E\Phi_{E_{prec}}(E)\,dE .$$

The equations derived above are expressed in SI units and should be multiplied with the appropriate scaling factor for use with variables expressed in different units.

The precipitated differential energy spectrum $\Phi_{E_{prec}}(E)$ can be used to infer the electron lifetimes in a given magnetic flux tube subject to certain assumptions as discussed below. We note in this context that the precipitated differential energy spectrum may change as a function of time both because of temporal changes in the ambient flux or because of variations in the parameters of the wave interacting with the electrons. For the purpose of estimating electron lifetimes $\tau(E)$, we assume that the precipitated differential energy spectrum remains constant in time, i.e.,

$$\Phi_{E_{prec}}(E,t) \cong \Phi_{E_{prec}}(E) .$$

We define N_f as the number of energetic electrons with a given energy per unit energy in a flux tube, per unit area of a tube cross section, at the equator so that the SI unit of the variable N_f is electrons m^{-2} J^{-1}. We assume that N_f decays exponentially in time as a result of the resonant scattering due to the electron–wave interaction

$$N_f(E,t) = N_f(E)e^{-\frac{t}{\tau(E)}}$$

while

$$\frac{\partial N_f(E,t)}{\partial t} = -\Phi_{E_{prec}}(E,t) = -\Phi_{E_{prec}}(E)$$

so that the lifetime of the electrons in a given tube is

$$\tau(E) = \frac{N_f(E)}{\Phi_{E_{prec}}(E)} .$$

Table 1. Parameters of Nonducted Waves

L	N_e, electrons cm^{-3}	f, kHz	$\psi(\lambda)$, deg
2	1500	2.6	$\psi = 90 - 0.0684\sqrt{8^2 - (\lambda - 0.15)^2}$
3	600	0.78	$\psi = 90 - 0.07\sqrt{6^2 - (\lambda - 0.1)^2}$
4	400	0.33	$\psi = 90 - 0.0727\sqrt{5.5^2 - (\lambda - 0.1)^2}$

The dependence of the wave normal angle on geomagnetic latitude and the frequency of oblique whistler mode waves which settle down on the corresponding L shell. Also given are the equatorial cold electron densities assumed for each of the corresponding L shells.

Note that the electron lifetimes defined above are derived for the electron population confined to a narrow flux tube around the field line where the interaction takes place. The extent to which this loss process contributes to the electron lifetimes on a global scale depends on the extent of magnetospheric regions illuminated by the waves, since similar scattering processes would be expected in all regions where the oblique waves are present. Experimental data indicate that magnetospheric regions illuminated by whistlers from a given thunderstorm center may extend to many tens of degrees in longitude around that of the storm center [*Sonwalkar and Inan*, 1993].

6. Electron Precipitation by MR Whistlers

We now investigate the interaction between radiation belt electrons and MR whistlers in the equatorial region at three typical L shells. The Poynting flux of the whistler waves was assumed to be $S = 113$ pWm^{-2} corresponding to the intensity of a $f = 6.82$ kHz ducted wave ($\psi = 0°$) with $B_w = 5$ pT in the equatorial plane at $L = 4$. The frequencies of the waves that settle down at the chosen L shells and the dependence of their wave normal angle ψ on the geomagnetic latitude are determined using the Stanford raytracing simulation code, and are given in Table 1. The $\psi(\lambda)$ represents best fits to the numerical results obtained from ray tracing. The variation of wave normal angle along the field line $\psi(\lambda)$ is slow enough so that the wave can be considered monochromatic in the WKB sense. The maximum change of wave normal angle ψ during the course of one electron gyroperiod occurs for the high electron energies for which the resonant interaction occurs in the region of the most rapid change of wave parameters cosidered (see Table 2). Using the expressions for $\psi(\lambda)$ from Table 1, the value of maximum change of wave normal angle during the course of one electron gyroperiod is calculated to be of the order of $10^{-3°}$.

We now study the resonant interaction between these monochromatic MR signals and radiation belt electrons represented by the distribution function as defined earlier, using the test particle simulation model.

Table 2 defines the boundaries of the regions in the velocity space, the cell sizes, and the region along the field line included in our model for all three L shells considered.

Single test particle trjectories were examined to determine the region in velocity space that includes all electrons that can resonantly interact with the chosen wave and that could be scattered into the loss cone. The minimum value of the initial equatorial pitch angle is equal to the loss cone angle for the appropriate L shell. At $L = 3$, for example $\min(\alpha_{eq_{init}}) = \alpha_{eq_{lc}}(L = 3) = 8.62019°$. The maximum value of the initial pitch angle and the cell size $\Delta\alpha_{eq}$ were determined by the maximum pitch angle scattering. We choose the upper limit of the simulated region such that all the electrons that could possibly have their pitch angles lowered to $\alpha_{eq} < \alpha_{eq_{lc}}$ in a single encounter with the wave are included, that is $\max(\alpha_{eq_{init}}) = \min(\alpha_{eq_{init}}) + 2\max(\Delta\alpha_{eq_{scatt}})$. The smaller the step size, the better resolution of the fine structure of distribution function dependence on velocity space coordinates. However, the cell size $\Delta\alpha_{eq}$ cannot be smaller than the fluctuation or 'noise' level of electron pitch angle change oscillations ($\Delta\alpha_{eq\ noise} \cong 10^{-4°}$, see Figure 9). In general, the distribution function after a one–pass interaction does not depend significantly on the pitch angle; instead, the fine structure of this distribution function depends strongly on $v_{z_{eq}}$ (Figure 12). We choose the pitch angle cell size to be $\Delta\alpha_{eq} = 1 \times 10^{-5} - 6 \times 10^{-5°}$ so that the population of electrons that is being scattered into the loss cone is represented by 12-20 cells (see Table 2).

Electrons are considered to be in resonance with the wave when their velocity parallel to B_o is such that

$$v_z \simeq (\epsilon\omega_H - \omega)k_z^{-1} = v_R$$

where $\epsilon = \sqrt{1 - (v/c)^2}$, v is the total particle velocity, c is the speed of light, $k_z = (\omega/c)n\cos\psi$ is the wave vector along B_o, ω_H is the electron gyrofrequency, ω is the wave frequency, n is the refractive index and ψ is the wave normal angle. The value of the lower limit of $v_{z_{eq}}$ is smaller than the equatorial resonant velocity $v_R(\lambda = 0°)$ and was chosen such that all electrons whose pitch angle scattering due to the resonant interaction with the wave is larger than the noise scattering due to the nonresonant interaction with the

Table 2. Simulation Parameters

L	$v_{z_{eq}}, 10^6 m\ s^{-1}$	$\Delta v_{z_{eq}}$	α_{eq}, deg	$\Delta\alpha_{eq}$	λ, deg
2	270.0-283.1	0.05	16.76813-16.76827	1×10^{-5}	-7 to +7
3	220.8-261.1	0.1	8.62019-8.62043	2×10^{-5}	-5 to +4
4	186.6-215.0	0.1	5.4735-5.4747	6×10^{-5}	-4.5 to +5

Limits for the simulated region in velocity space, cell sizes, and constraints on the position of the resonant interaction along the L shell for the resonant interaction with the MR whistler mode waves settling down at $L = 2, 3, 4$.

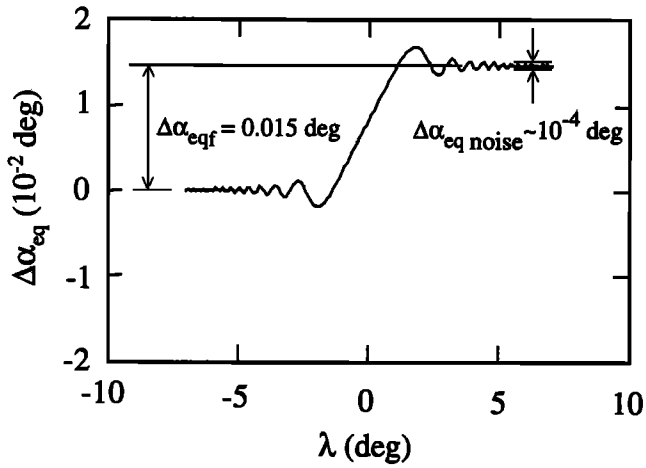

Figure 9. Noise scattering. On a sample test electron trajectory, we show resonant pitch angle scattering due to the interaction with the wave ($\delta\alpha_{eq}$), and oscillations in pitch angle change far away from the resonant interaction region that we refer to as noise scattering ($\delta\alpha_{eqnoise}$).

wave (e.g., $v_{z_{eq}} \ll v_R(\lambda = 0°)$), are included (Figure 9). After it reaches the maximum value (for $v_{z_{eq}}$ slightly higher than $v_R(\lambda = 0°)$), the rms value of the pitch angle change $\overline{\Delta\alpha_{eq_f}}$ decreases rapidly to the 'noise' level with the decrease in $v_{z_{eq}}$. (Example in Figure 10 is given for the interaction with MR whistler at $L = 3$.) These curves, obtained by examination of single test particle trajectories, were used to detemine $\min(v_{z_{eq}})$. The upper limit for $v_{z_{eq}}$ is determined by the constraint on validity of our simulation model, that is, that resonant interaction has to take place at a magnetic latitude where wave parameters do not change significantly over one gyroperiod in the reference frame of the electron. Figures 11 and Figures 12 show the dependence of electric and magnetic fields as well as the refractive index and wave group velocity on latitude for a wave that settles down at $L = 4$. Wave parameters change relatively more rapidly with geomagnetic latitude for $\lambda < -4.5°$ and $\lambda > 5°$, so at $L = 4$ we choose to consider resonant interactions of the given wave with near-loss-cone radiation belt electrons with energy such that $v_{z_{eq}} < \max(v_{z_{eq}}) = \min[v_R(\lambda = -4.5°), v_R(\lambda = 5°)]$.

We choose velocity cell size $\Delta v_{z_{eq}}$ such that the fine structure of electron pitch angle scattering dependence on $v_{z_{eq}}$ (see Figure 10) is preserved. For the cases considered, $\Delta v_{z_{eq}} = 5 \times 10^4 - 1 \times 10^5$ m/s.

Figure 13 shows the near-loss-cone electron distribution function resulting from a one–pass interaction with a 0.33 kHz oblique whistler wave at $L = 4$. Local maxima and minima in electron scattering occur due to the constructive and destructive interference between the two resonant encounters (on both sides of the equator) of the particles with the wave that occur for $v_{z_{eq}} > v_R(\lambda = 0°)$. Maximum penetration into the loss cone ($\sim 5 \times 10^{-4}$°) occurs for $v_{z_{eq}} = 198.4 \times 10^6$m s^{-1}, which is slightly higher (2.96%) than $v_R(\lambda = 0°) = 192.7 \times 10^6$m s^{-1}.

The distribution functions similar to that shown in Figure 13 and which result from a one–pass interaction with the wave are also computed for $L = 2$ and 3 and are subsequently used to calculate the precipitated differential electron spectra as shown in Figure 14 for all three L shells. In general, MR whistler components which settle down on higher L shells resonantly interact with and scatter lower-energy electrons. For example, a 0.33 kHz whistler wave at $L = 4$ scatters electrons in the 150–220 keV range, whereas the 2.6 kHz MR whistler component that settles down at $L = 2$ scatters electrons in the 1–2 MeV energy range. Precipitated differential electron flux is in general higher for lower energy electrons that are scattered on higher L shells. The maximum value of the precipitated differential electron flux at $L = 4$ is $\Phi_{E_{prec}}(173 \text{ keV}) = 4.6 \times 10^{-1}$ electrons cm^{-2} s^{-1} keV^{-1}. The corresponding total precipitated energy fluxes are

$$Q(L = 2) = 0.48 \times 10^{-9} \frac{\text{J}}{\text{m}^2\text{s}} = 0.48 \times 10^{-6} \frac{\text{erg}}{\text{cm}^2\text{s}}$$

$$Q(L = 3) = 2.66 \times 10^{-9} \frac{\text{J}}{\text{m}^2\text{s}}$$

$$Q(L = 4) = 3.14 \times 10^{-9} \frac{\text{J}}{\text{m}^2\text{s}}$$

and are generally higher for higher L shells.

It can be seen in Figure 14 that the precipitated flux at $L = 4$ shows much larger variability with particle energy than that at $L = 2$ and 3. This occurs because the wave refractive index is generally larger at $L = 4$, and for these larger values the scattering efficiency of the MR wave is a strong function of particle energy. This type of variability is discussed by *Bell* [1984].

The electron lifetimes corresponding to the precipitated fluxes of Figure 14 and calculated using the definitions and assumptions described earlier are given as a function of electron energy in Figure 15. The minimum lifetimes of the electrons with the corresponding energy that are scattered by MR whistlers are of the order of several days and do not differ significantly for interactions on different L shells. The minimum electron lifetimes vary from 2.47 days for $E = 1.11$ MeV electrons at $L = 2$ to 4.64 days for $E = 173$ keV electrons at $L = 4$.

In Figure 16 we compare our lifetime estimates with those due to cyclotron resonant scattering by whistler mode hiss

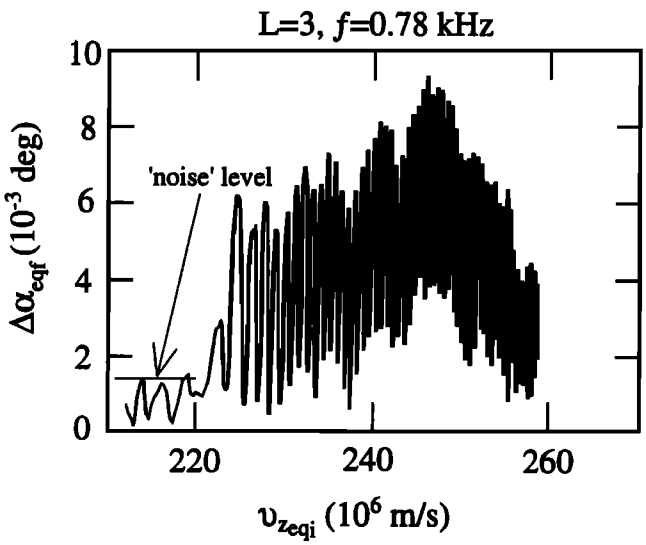

Figure 10. Dependence of particle scattering on initial uzeq. The root-mean-square value of the particle pitch angle change is plotted for different initial electron velocities uzeq. Pitch angle scattering depends strongly on uzeq with local maxima and minima corresponding respectively to the constructive and destructive interference between the two resonant encounters of the particles with the wave. With the decrease in uzeq, scattering eventually reaches the noise level (Figure 9).

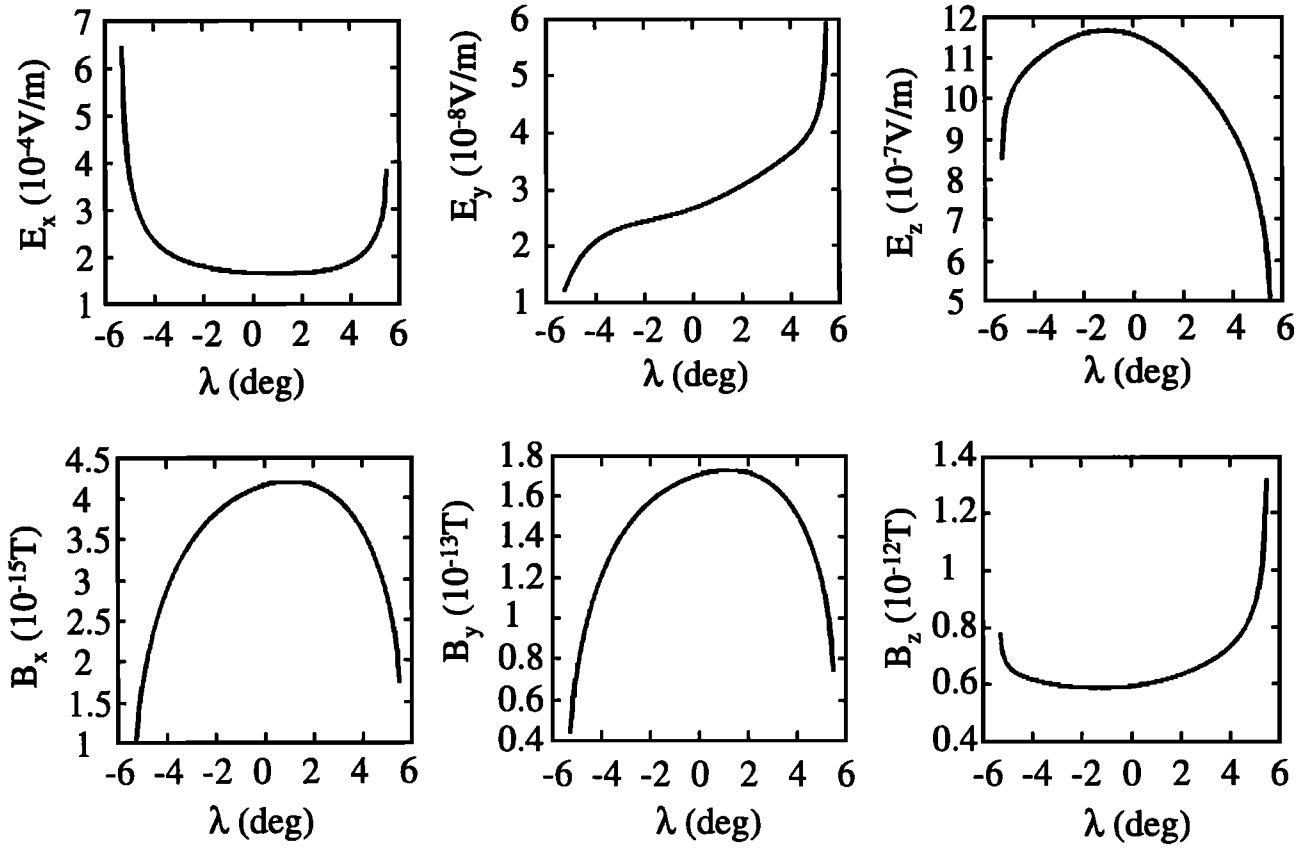

Figure 11. Dependence of the wave parameters on geomagnetic latitude along the field line. For a 0.33 kHz whistler mode wave that settles down at $L \equiv 4$, best fit to the numerical data from the raytracing was used to determine the wave normal angle dependence on geomagnetic latitude $\psi(\lambda)$ along the $L = 4$ field line. For such a wave, the dependence of wave electric (E_x, E_y, E_z) and magnetic $(B_x, B_y B_z)$ fields on latitude λ, at $L = 4$ is given.

following large magnetic storms [*Lyons et al.*, 1972]. Interaction between radiation belt electrons and hiss causes precipitation and loss from $L = 3$ and 4 of electrons in a broader energy range than that due to the resonant electron–MR whistler interaction. At $L = 3$ and 4, electron lifetimes due to hiss induced losses are smaller than the electron lifetimes due to resonant electron–MR whistler interaction. However, at $L = 2$, MR whistlers can contribute more than hiss to the electron loss from the radiation belts. Note that the results given by *Lyons et al.* [1972] are calculated based on the assumption of the continuous presence of a wide band oblique whistler mode signal throughout the entire plasmasphere. In order to be able to compare the two, we also assumed the continuous presence of coherent, narrowband oblique whistler mode signal throughout the entire plasmasphere. However, our results can be scaled to more realistic

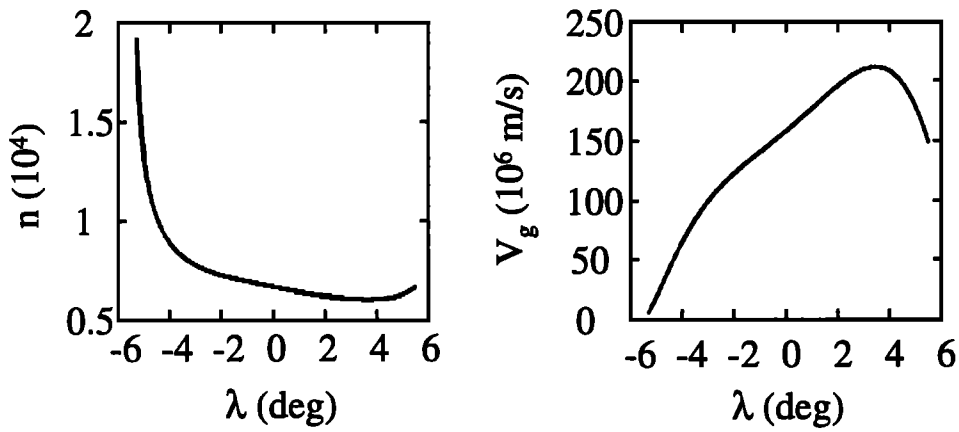

Figure 12. Dependence of the wave refractive index n and group velocity V_g on latitude λ at $L = 4$ under the conditions described in Figure 11.

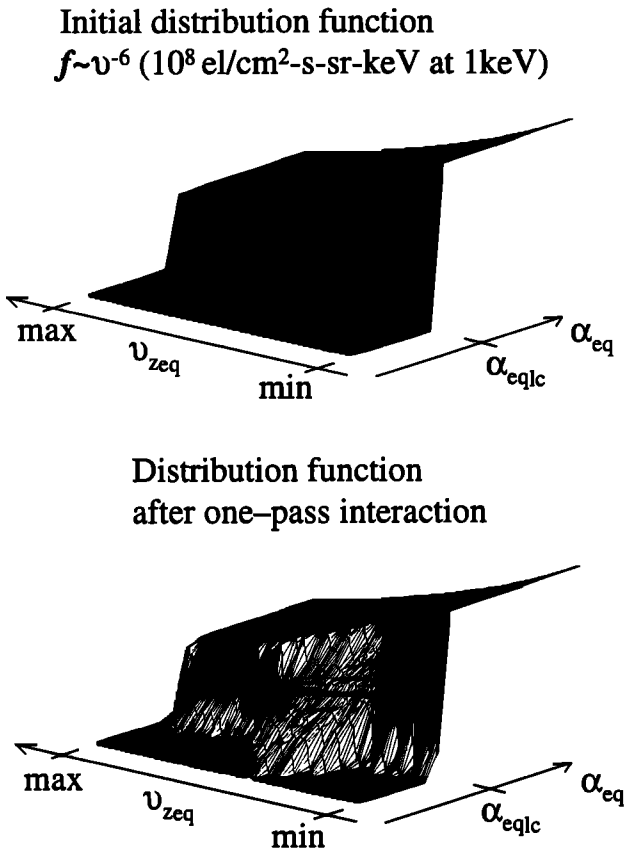

Figure 13. The initial and final near loss cone electron distributions for a one pass interaction with a 0.33 kHz whistler wave at $L = 4$. Local maxima and minima in electron scattering occur due to the constructive and destructive interference between the two resonant encounters of the distribution with the wave.

values by simple multiplication once the ratios for spatial and temporal presence of the MR whistlers throughout the plasmasphere are available.

7. Conclusions

We have carried out test particle simulations of the cyclotron resonant scattering of radiation belt electrons in a single resonant encounter (one pass) with obliquely propagating monochromatic whistler mode waves in the magnetosphere. Our results indicate that for typical parameters as used in this paper, these interactions result in significant perturbations of the trapped particle distributions and lead to precipitation of particle fluxes into the ionosphere. Although our individual simulations were limited to one–pass interactions with monochromatic oblique waves, when viewed as a whole, they imply that wave energy injected into the magnetosphere by lightning and propagating obliquely in the nonducted mode may substantially contribute to the establishment of radiation belt equilibrium.

In this context, we have shown that oblique MR waves which settle down on given L shells and exist for up to 100 s can significantly affect the lifetimes of the energetic electrons. In the case of the latter, it should be noted that nonducted whistlers injected into the magnetosphere typically have components over a wide range of frequencies, so that each frequency component would 'settle' on a different L shell and the scattering (as computed) can be expected to

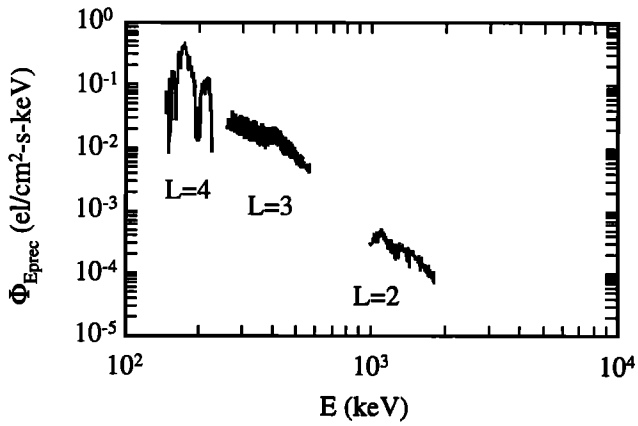

Figure 14. Precipitated differential electron spectra. For all three cases considered, precipitated differential electron spectra is calculated from the distribution function (such as that in Figure 12) after a one pass interaction with the corresponding wave.

occur simultaneously over a broad range of L shells during the 10–100 s following each lightning discharge.

The implications of our results should be evaluated in the context of recent theoretical and experimental findings which clearly indicate that ducted whistler waves originating in lightning regularly precipitate energetic radiation belt electrons. The ionospheric signatures of the scattering of energetic electrons out of the radiation belts in cyclotron resonant interactions with lightning–generated ducted (i.e., parallel propagating) whistlers has been both theoretically studied in detail [*Inan*, 1977; *Inan et al.*, 1982; *Chang*, 1983; *Chang and Inan*, 1983b; *Chang and Inan*, 1985] and commonly observed [*Inan et al.*, 1990; *Burgess and Inan*, 1990, and references therein]. As a measure of the effectiveness of this interaction, precipitated energetic electron fluxes have been theoretically estimated and compared with experimental data [*Inan et al.*, 1985b; *Inan and Carpenter*, 1987]. Although ducted whistlers often reflect from the lower ionospheric boundary and can bounce back and forth along the duct multiple times, most experimental evidence of ducted whistler induced precipitation involves single encounter interactions with a discrete one–hop whistler.

However, the bulk of the magnetospheric wave energy from lightning discharges propagates in the nonducted mode.

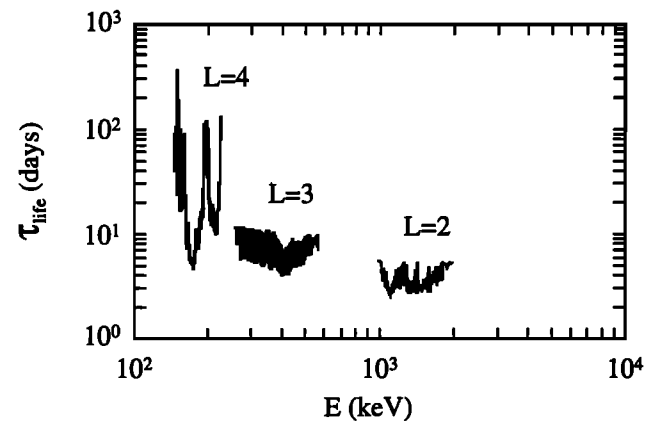

Figure 15. Electron lifetimes. Precipitated differential electron spectra are used to calculate electron lifetimes as discussed in the text.

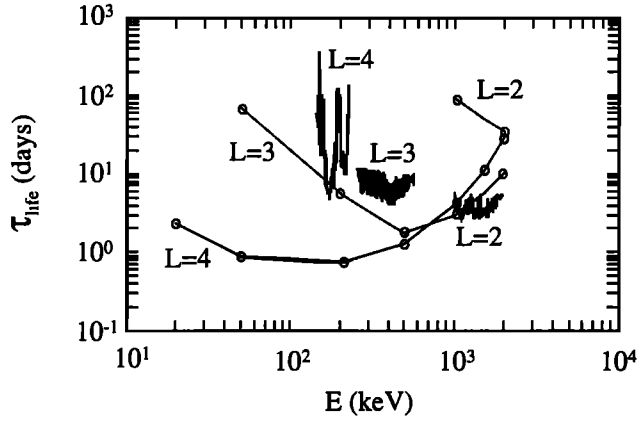

Figure 16. Electron lifetimes compared with previous work. We compare our lifetime estimates (solid curve) with those due to cyclotron scattering by whistler mode hiss following large magnetic storms [Lyons et al., 1972] (curve with circles).

Nonducted whistlers do not require the presence of any specific density structures (e.g., ducts) for their propagation, and they generally occupy larger regions of the magnetosphere (V. S. Sonwalkar and U. S. Inan, Thunderstorm coupling to the magnetosphere, submitted to *Journal of Geophysical Research*, 1998). On this basis, although the statistics of the occcurrence rates of nonducted whistlers are not well documented, it may safely be assumed that they occur at least as often as ducted whistlers and may well be excited by every lightning discharge.

Interaction of radiation belt electrons with MR whistlers at a later stage of their propagation (after the settlement of ray paths on a certain L shell, when the wave normal angle is high, close to 90°) endures for as long as the waves exist (~100 s) so that it is appropriate to discuss the consequences of the losses in terms of radiation belt electron lifetimes. Interactions with MR whistlers causes precipitation of higher-energy electrons from lower L shells. Electrons in the energy range of 1–2.6 MeV are precipitated from $L = 2$, whereas from $L = 4$ precipitated electron energy range is 150–220 keV. The precipitated differential electron flux, due to this interaction, is higher for higher L shells, and the maximum value is ranging from $\Phi_{E_{prec}}(1.11\ \text{MeV}) = 5.2 \times 10^{-4}$ electrons cm^{-2} s^{-1} keV^{-1} at $L = 2$ to $\Phi_{E_{prec}}(173\ \text{keV}) = 4.6 \times 10^{-1}$ electrons cm^{-2} s^{-1} keV^{-1} at $L = 4$. The lifetimes of the radiation belt electrons in a tube around the L shell on which the interaction takes place range depending on electron energy from several days to ~100 days and are comparable with lifetimes corresponding to electron loss induced by hiss [*Lyons et al.*, 1972]. The minimum electron lifetimes vary from 2.47 days for $E = 1.11$ MeV electrons at $L = 2$ to 4.64 days for $E = 173$ keV electrons at $L = 4$.

Acknowledgments. This work was supported by NASA grant NAG5-4554-1 and by NASA GSFC grant NAS5-30371 (under subcontract to the University of Iowa).

The Editor thanks T. J. Rosenberg and A. J. Smith for their assistance in evaluating this paper.

References

Angerami, J. J., and J. O. Thomas, Studies of planetary atmospheres, 1, The distribution of electrons and ions in the Earth's exosphere, *J. Geophys. Res., 69*, 4537, 1964.

Bell, T. F., The nonlinear gyroresonance interaction between energetic electrons and coherent VLF waves propagating at an arbitrary angle with respect to the Earth's magnetic field, *J. Geophys. Res., 89*, 905, 1984.

Bell, T. F., U. S. Inan, and R. A. Helliwell, Nonducted coherent VLF waves and associated triggered emissions observed on the ISEE-1 satellite, *J. Geophys. Res., 86*, 4649, 1981.

Burgess, W. C., and U. S. Inan, Simultaneous disturbance of conjugate ionopheric regions in association with individual lightning flashes, *Geophys. Res. Lett., 17*, 259, 1990.

Burgess, W. C., and U. S. Inan, The role of ducted whistlers in the precipitation loss and equilibrium flux of radiation belt electrons, *J. Geophys. Res., 98*, 15,643, 1993.

Carlson, C. R., R. A. Helliwell, and U. S. Inan, Space–time evolution of whistler mode wave growth in the magnetosphere, *J. Geophys. Res., 95*, 15,073, 1990.

Carpenter, D. L., and J. W. LaBelle, A study of whistlers correlated with bursts of electron precipitation near $L = 2$, *J. Geophys. Res., 87*, 4427, 1982.

Chang, C. H., Cyclotron resonant scattering of energetic electrons by electromagnetic waves in the magnetosphere, *Tech. Rep. E414-1*, STARLAB, Stanford Electron. Lab., Stanford Univ., Stanford, Calif., 1983.

Chang, C. H., and U. S. Inan, Quasi–relativistic electron precipitation due to interactions with coherent VLF waves in the magnetosphere, *J. Geophys. Res., 88*, 318, 1983a.

Chang, H. C., and U. S. Inan, A theoretical model study of observed correlations between whistler mode waves and energetic electron precipitation events in the magnetosphere, *J. Geophys. Res., 88*, 10,053, 1983b.

Chang, H. C., and U. S. Inan, Lightning–induced electron precipitation from the magnetosphere, *J. Geophys. Res., 90*, 1531, 1985.

Chang, H. C., U. S. Inan, and T. F. Bell, Energetic electron precipitation due to gyroresonant interactions in the magnetosphere involving coherent VLF waves with slowly–varying frequency, *J. Geophys. Res., 88*, 7037, 1983.

Dingle, B., and D. L. Carpenter, Electron precipitation induced by VLF noise bursts at the plasmapause and detected at conjugate ground stations, *J. Geophys. Res., 86*, 4597, 1981.

Draganov, A. B., U. S. Inan, V. S. Sonwalkar, and T. F. Bell, Magnetospherically reflected whistlers as a source of plasmaspheric hiss, *Geophys. Res. Lett., 19*, 233, 1992.

Dungey, J. W., Loss of Van Allen electrons due to whistlers, *Planet. Space Sci., 11*, 591, 1963.

Edgar, B. C., The upper and lower frequency cutoffs of magnetically reflected whistlers, *J. Geophys. Res., 81*, 205, 1976.

Foster, J. C., and T. J. Rosenberg, Electron precipitation and VLF emissions associated with cyclotron resonance interactions near the plasmapause, *J. Geophys. Res., 81*, 2183, 1976.

Helliwell, R. A., A theory of discrete VLF emissions from the magnetosphere, *J. Geophys. Res., 72*, 4773, 1967.

Helliwell, R. A., VLF stimulation experiments in the magnetosphere from siple station, Antarctica, *Rev. Geophys., 26*, 551, 1988.

Helliwell, R. A., and J. P. Katsufrakis, VLF wave injection into the magnetosphere from Siple Station, Antartica, *J. Geophys. Res., 79*, 2511, 1974.

Helliwell, R. A., J. P. Katsufrakis, and M. L. Trimpi, Whistler-induced amplitude perturbation in VLF propagation, *J. Geophys. Res., 78*, 4679, 1973.

Helliwell, R. A., S. B. Mende, J. H. Doolittle, W. C. Armstrong, and D. L. Carpenter, Correlations between λ4278

optical emissions and VLF wave events observed at $L \sim 4$ in the Antarctic, *J. Geophys. Res., 85*, 3376, 1980.

Inan, U. S., Non-linear gyroresonant interactions of energetic particles and coherent VLF waves in the magnetosphere, *Tech. Rep. 3414-3*, Radiosci. Lab., Stanford Electron. Lab., Stanford Univ., Stanford, Calif., 1977.

Inan, U. S., Gyroresonant pitch angle scattering by coherent and incoherent whistler mode waves in the magnetosphere, *J. Geophys. Res., 92*, 127, 1987.

Inan, U. S., and T. F. Bell, The plasmapause as a VLF wave guide, *J. Geophys. Res., 82*, 2819, 1977.

Inan, U. S., and D. L. Carpenter, Lightning-induced electron precipitation events observed at $L = 2.4$ as phase and amplitude perturbations on subionospheric VLF signals, *J. Geophys. Res., 92*, 3293, 1987.

Inan, U. S., T. F. Bell, and R. A. Helliwell, Nonlinear pitch angle scattering of energetic electrons by coherent VLF waves in the magnetosphere, *J. Geophys. Res., 83*, 3235, 1978.

Inan, U. S., T. F. Bell, and H. C. Chang, Particle precipitation induced by short-duration VLF waves in the magnetosphere, *J. Geophys. Res., 87*, 6243, 1982.

Inan U. S., D. L. Carpenter, R. A. Helliwell, and J. P. Katsufrakis, Subionospheric VLF/LF phase perturbations produced by lightning-whistler induced particle precipitation, *J. Geophys. Res., 90*, 7457, 1985a.

Inan, U. S., H. C. Chang, R. A. Helliwell, W. L. Imhof, J. B. Reagan, and M. Walt, Precipitation of radiation belt electrons by man-made waves: A comparison between theory and measurements, *J. Geophys. Res., 90*, 359, 1985b.

Inan, U. S., M. Walt, H. D. Voss, and W. L. Imhof, Energy spectra and pitch angle distributions of lightning-induced electron precipitation: analysis of an event observed on the S81-1 (SEEP) satellite, *J. Geophys. Res., 94*, 1379, 1989.

Inan, U. S., F. A. Knifsend, and J. Oh, Subionospheric VLF "imaging" of lightning-induced electron precipitation from the Mmagnetosphere, *J. Geophys. Res., 95*, 17217, 1990.

Jasna D., U. S. Inan, and T. F. Bell, Precipitation of suprathermal (100 eV) electrons by oblique whistler waves, *Geophys. Res. Lett., 19*, 1639, 1992.

Kennel, C. F., and H. E. Petschek, Limit on stably trapped particle fluxes, *J. Geophys. Res., 71*, 1, 1966.

Laaspere, T., W. C. Johnson, and L. C. Semprebon, Observations of auroral hiss, LHR noise, and other phenomena in the frequency range 20 Hz - 540 kHz on OGO 6, *J. Geophys. Res., 76*, 4477, 1971.

Lohrey, B., and A. B. Kaiser, Whistler-induced anomalies in VLF propagation, *J. Geophys. Res., 84*, 5122, 1979.

Lyons, L. R., and R. M. Thorne, Equilibrium structure of radiation belt electrons, *J. Geophys. Res., 78*, 2142, 1973.

Lyons, L. R., R. M. Thorne, and C. F. Kennel, Electron pitch-angle diffusion driven by oblique whistler-mode turbulence, *J. Plasma Phys., 6*, 589, 1971.

Lyons, L. R., R. M. Thorne, and C. F. Kennel, Pitch-angle diffusion of radiation belt electrons within the plasmasphere, *J. Geophys. Res., 77*, 3455, 1972.

Mende, S. B., R. M. Arnoldy, L. J. Cahill Jr., J. H. Doolittle, W. C. Armstrong, and A. C. Fraser-Smith, Correlation between λ4278-A optical emissions and a Pc 1 pearl event observed at siple station, Antarctica, *J. Geophys. Res., 85*, 1194, 1980.

Park, C. G., Methods of determining electron concentrations in the magnetosphere from nose whistlers, *Tech. Rep. 3454-1*, Radioscience Laboratory, Stanford Electron. Lab., Stanford Univ., Stanford, Calif., 1972.

Roberts, C. S., Electron loss from the Van Allen zones due to pitch angle scattering by electromagnetic disturbances, in *Radiation Trapped in the Earth's Magnetic Fields*, edited by B. M. Mc Cormac, P. D. Reidel, Norwell, Mass., 1966.

Roberts, C. S., Pitch-angle diffusion of electrons in the magnetosphere, *Rev. Geophys., 7*, 305, 1969.

Rosenberg, T. J., R. A. Helliwell, and J. P. Katsufrakis, Electron precipitation associated with discrete very-low-frequency emissions, *J. Geophys. Res., 76*, 8445, 1971.

Rosenberg, T. J., J. C. Siren, D. L. Mathews, K. Marthinsen, J. A. Holtet, A. Egeland, D. L. Carpenter, and R. A. Helliwell, Conjugacy of electron microbursts and VLF chorus, *J. Geophys. Res., 86*, 5819, 1981.

Schield, M. A., and L. A. Frank, Electron observations between the inner edge of the plasma sheet and the plasmasphere, *J. Geophys. Res., 75*, 5401, 1970.

Spjeldvik, W. N., and R. M. Thorne, The cause of storm after effects in the middle latitude D-region, *J. Atmos. Terr. Phys., 37*, 777, 1975.

Stix, T. H., *The Theory of Plasma Waves*, McGraw-Hill, New York, 1962.

Thorne, R. M., and R. B. Horne, Landau damping of magnetospherically reflected whistlers, *J. Geophys. Res, 99*, 17249, 1994.

Tsurutani, B. T., and E. J. Smith, Postmidnight chorus: A substorm phenomenon, *J. Geophys. Res., 79*, 118, 1974.

T. F. Bell and U. S. Inan, STAR Laboratory, Stanford University, Durand 315, Stanford, CA 94305-9515.

J. L. Ristić-Djurović, Vinča Institute of Nuclear Science, Belgrade, Yugoslavia (E-mail: edjurovj@etf.bg.ac.yu).

(Received September 5, 1997; revised December 18, 1997; accepted December 18, 1997.)